ISET Journal of Earthquake Technology, Paper No. 493, Vol. 44, No. 3-4, Sept.-Dec. 2007, pp. 421–444

SEISMIC PERFORMANCE AND FINANCIAL RISK OF MASONRY HOUSES

J.K. Bothara*, J.B. Mander**, R.P. Dhakal***, R.K. Khare**** and M.M. Maniyar****

*Beca Carter Hollings & Ferner Ltd., Wellington, New Zealand

**Zachry Department of Civil Engineering, Texas A&M University, College Station, Texas, U.S.A.

***Department of Civil Engineering, University of Canterbury, Private Bag 4800, Christchurch, New Zealand

****Department of Civil Engineering, S.G.S. Institute of Technology & Science, Indore-452003

ABSTRACT

Seismic behaviour of a typical unreinforced masonry (URM) brick house is experimentally investigated. A half-scale URM house model with aspect ratio of 1.5:1 in plan is constructed and tested on a shaking table, in the longitudinal direction for several earthquake ground motions with peak ground acceleration (PGA) up to 0.5*g*. The structure is then rotated by 90º and tested in the transverse (short) direction for ground motions with PGA up to 0.8*g*. A finite element analysis and a mechanism analysis are conducted to assess the dynamic properties and lateral strength of the model house. Seismic fragility function of the URM houses is developed based on the experimental results. Damping at different phases of the response is estimated by using an amplitude-dependent equivalent viscous damping model. Financial risk of similar URM houses is then estimated in terms of expected annual loss (EAL) by following a probabilistic financial risk assessment framework. Risks posed by different levels of damage and by earthquakes of different predominant frequencies are then examined.

KEYWORDS: Unreinforced Masonry (URM), Seismic Performance, Fragility, Expected Annual Loss (EAL), Hazard Survival Probability

INTRODUCTION

Dynamic tests of unreinforced masonry (URM) buildings and wall components have been conducted in different parts of the world in order to investigate rehabilitation requirements of such buildings. Tomazevic (1987) tested dynamically a one-seventh scaled, four-storey, unreinforced brick masonry building model. His model possessed a reinforced concrete rigid floor diaphragm and masonry piers from floor to the ceiling height. Since all the damage was observed in the first storey, he recommended a storey mechanism model for the analysis of such buildings. He also tested three 1:4 scale two-storey house models, constructed in brick laid in cement, lime and sand mortar and with timber floors, representing old historic houses (Tomazevic, 1996). The models were constructed with and without roof ties to investigate and compare the effects of these ties on the seismic behaviour of such buildings. He concluded that the behaviour of URM houses depended on the rigidity of the floor diaphragm and the connection between the diaphragm and the walls. Qamaruddin and Chandra (1991) conducted shaking table tests of small-scale URM building models. They reported that the walls supporting floor/roof suffer more damage if the shaking is normal to them unless the strength of in-plane walls is mobilised through the diaphragm action.

Response of an instrumented two-story URM shear wall building with flexible diaphragms has been reported previously by Tena-Colunga and Abrams (1992). This triggered a whole series of experimental investigations on URM houses with flexible floor diaphragms. Calvi and Pavese (1995) conducted full-scale tests on a two-storey brick masonry model with flexible floor diaphragms to explore dynamic parameters and failure mechanisms in URM buildings. Costley and Abrams (1996) reported tests of two 3/8-scale models, constructed in brick with cement, lime and sand mortar with flexible floor and roof, to explore simplified methods for evaluation and rehabilitation of URM buildings. Benedetti and Pezzoli (1996) conducted a comprehensive study to investigate the behaviour of URM buildings before and after seismic intervention. They reported testing of 24 half-scale URM building models, constructed of brick or stone in lean mortar and with flexible floor and roof, representing existing masonry buildings. Recently, Peralta et al. (2002) investigated the seismic performance of rehabilitated floor and roof diaphragms in the URM buildings of pre-1950s, and Yi et al. (2006a, 2006b) conducted experimental and analytical investigations on the seismic behaviour of a two-storey URM building.

In addition to the above-mentioned dynamic testing of three-dimensional models, dynamic tests have been conducted on URM components as well to investigate their seismic performance. Magenes and Calvi (1995) conducted dynamic tests on eight URM walls to scrutinize the influence of parameters such as mortar strength and aspect ratio on in-plane failure modes, and compared the results with those of quasi-static tests conducted on similar specimens. They found good correlation between the dynamic and quasi-static test results in terms of failure mechanism and interaction of fundamental parameters. Doherty (2000) and Simsir et al. (2003) have reported dynamic testing of scaled URM masonry walls conducted to investigate their out-of plane behaviour. They concluded that the out-of-plane collapse of URM walls is primarily associated with excessive displacement rather than attainment of static out-of-plane strength of the walls.

Increasing interest in the last few decades in masonry construction has resulted in research and prescription of seismic vulnerability assessment methodologies for URM buildings. For this purpose, visual assessment methods are prescribed by several sources such as FEMA 154 (FEMA, 1988), Sobaih (1999), and NSET (2000). Detailed assessment methods are given by Arya (1992), NZSEE (1995, 2006), FEMA 356 (FEMA, 2000), and Tomazevic (1999). Magenes (2000) has given a more comprehensive description of an assessment procedure of URM buildings based on the preceding work by Magenes and Calvi (1999). The study conducted by Moon et al. (2006) has led to recommendations for seismic evaluation and retrofit of low-rise URM structures.

For the out-of-plane vulnerability assessment of URM walls, Priestley (1985) proposed a velocity-based approach based on equal-energy principle, while considering the energy balance of the responding walls and reserve capacity of the rocking walls. However, in this method the energy demand is very sensitive to the selection of elastic natural frequency. Lately, a displacement-based approach has been proposed by various researchers including Doherty (2000), Doherty et al. (2002), Griffith et al. (2003), and Griffith and Magenes (2003). They have proposed a tri-linear static force-displacement relationship for the seismic vulnerability assessment of out-of-plane walls. In particular, Griffith et al. (2003) predicted collapse by using "appropriate" stiffness and elastic response spectra and, in contrast to Priestley (1985), argued that the initial stiffness (thereby the initial period) is not crucial in determining the occurrence of collapse. De Felice and Giannini (2000, 2001) studied the out-of-plane resistance of masonry walls based on simple collapse mechanisms, and conducted numerical analysis taking into account the connection between the longitudinal and transverse walls. ATC 40 (ATC, 1996) proposed a new displacement-based seismic evaluation methodology based on the Capacity Spectrum Method for reinforced concrete buildings. This method utilizes the acceleration-displacement response spectrum (Mahaney et al., 1993) as demand curve, and pushover curve as the capacity curve. This has been used by Costley and Abrams (1996) to predict the in-plane capacity of unreinforced brick masonry building models.

The present work seeks to estimate financial loss through investigation of the dynamic performance of URM houses. In this context, a half-scale brick masonry house with a flexible floor and roof was dynamically tested on shaking table. This work investigates the deficiencies in URM houses and their effects on the overall seismic performance. Furthermore, it focuses on the development of an analytical method to generate fragility functions to predict the extent of damage in such houses at various levels of ground shaking during experiments. Fragility curves thus drawn are used to estimate the financial loss. The authors are aware of some studies that investigated the fragility of URM structures (Craig et al., 2002; Park et al., 2002; Towashiraporn et al., 2002), but none has extended fragility functions to the seismic loss assessment. An earthquake–recurrence relationship is defined to transform earthquake intensity to annual frequency. A loss ratio, which is the ratio of the cost necessary to restore the full functionality of the structure to the replacement cost, is then assigned to each damage state observed experimentally. Expected annual loss (EAL) is calculated using the extension of the Pacific Earthquake Engineering Research (PEER) Centre's triple integral formulation (Krawinkler and Miranda, 2004) by Dhakal and Mander (2005) to a quadruple integral equation. Limitations of the study and sensitivity to various parameters are reported. Comments useful to owners and insurers of the buildings are made from the insurance point of view.

EXPERIMENTAL INVESTIGATION

A two-storey half-scale URM house model was constructed and tested under earthquake ground motions on a shaking table. The one-room per floor house was constructed with clay brick masonry laid

in cement-lime-sand mortar. The house model had a conventional timber floor and timber frame roof clad with clay tiles. The openings like doors and windows were sized so that those represented a range of typical construction practices. The chosen model represents a generic non-engineered masonry house. Two examples of its prototype in Nepal and New Zealand are given in Bothara (2004). Due to the limitations of shaking table a length scale of one-half (i.e., 1:2) was adopted for this study. Thus, twin wythe walls were replicated in the model as a single wythe wall. The model was constructed with the same material as its prototype. By adopting constant-acceleration similitude, constant-stress and constant-strain similitudes are also achieved. This led to the following scale factors: force scale, S_F = 1/4; frequency scale, S_f = 1.414; time and velocity scales, S_t = S_v = 0.707; and mass density scale S_ρ = 2. The model structure with an aspect ratio of 1.5:1 in plan was initially tested in the longitudinal direction under several earthquake ground motions with PGA ranging up to 0.5*g*. The structure was then rotated by 90º and tested in the transverse (or short) direction under the ground motions with PGA in excess of 0.5*g*.

For the mass similitude, live loads were ignored. Additional masses of 120 kg, 1.97 t and 2.1 t were required at the gable walls, and floor and eaves levels, respectively. Out of the 120 kg of additional mass required, only 36 kg could be attached to each gable wall due to the space constraint and therefore the remaining mass was added at the floor level during the longitudinal testing. Thus, additional masses of 2.05 t and 2.09 t were added at the floor and eaves levels respectively. While testing in the transverse direction, the gable walls were not loaded with the additional load, and this load was added to that at the eaves level. To load the front and back walls, additional masses were fixed to the floor joists and roof ties. To load the side walls for stress simulation, platforms were constructed, one end of which was rigidly tied to the transverse walls while the other end rested on the sliding joints supported on the floor joists or roof ties.

1. Model Construction

The footprint of the 3.2 m high model was 2.88×1.92 m as shown in Figure 1. In constructing the model house, recycled full size "wire cut" bricks typical of early 1930s, known as the "seventy series", were used. Based on the customary building practices in the early last century a (cement : lime : sand) mortar mix of 1:1:6 was adopted. Coarse river sand comprising up to 3 mm particle size was used for the mortar, with hydrated lime and ordinary Portland cement used as binder. "Rimu", a native New Zealand wood, was used for the rafters and flooring material. For the rest of the woodwork, "Pinus Radiata" was used. A standard procedure was adopted in constructing the house model. During the construction of the house model, comprehensive tests were conducted to track mechanical properties of the masonry. Average values of those mechanical properties are presented in Table 1.

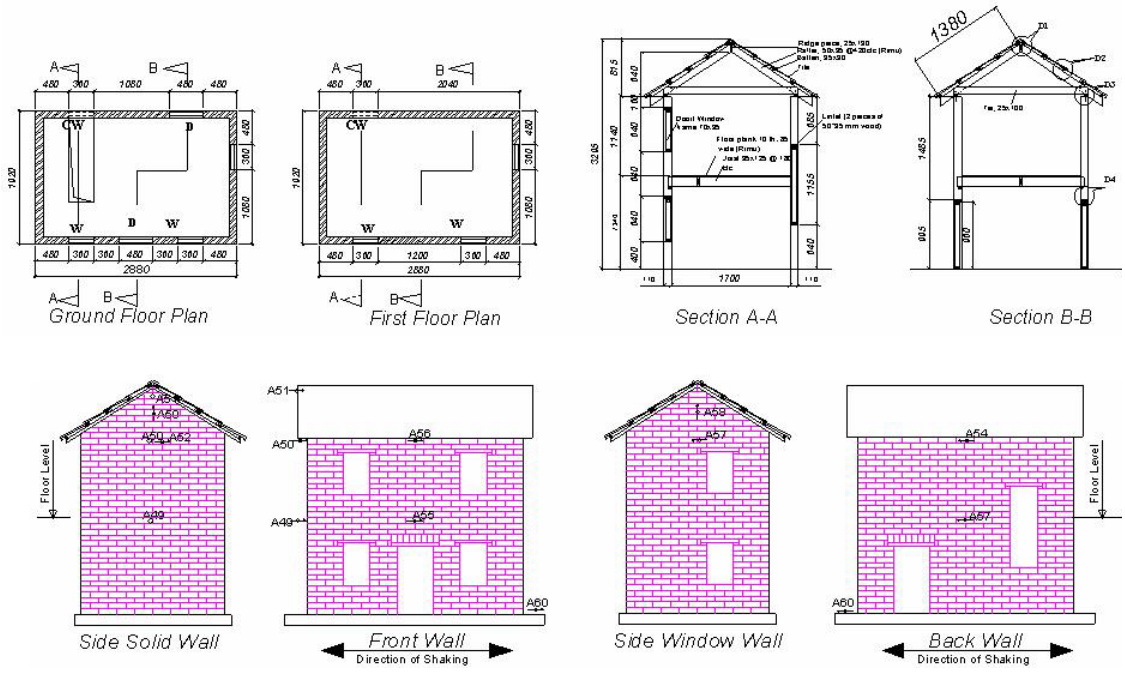

Fig. 1 Plan and elevation of the model

Table 1: Material Properties

Material	Test Type	Test Result	CoV	Remarks
Brick	Compressive Strength	26.6 MPa	17%	
	Initial Rate of Absorption (IRA)	63.6*g*	7.4%	
Mortar Cubes	Compressive Strength	7.6 MPa	10.6%	
Masonry Prism	Compressive Strength	16.2 MPa	19.7%	at 0.0035 strain
	Young's Modulus, *E*	6100 MPa	45.2%	at 0.0016 strain
	Shear Strength	τ_o = 0.93 MPa	38.6%	
		ϕ = 44.4º	13.4%	
	Flexural Bond	0.42 MPa	35%	
	Split Bond	0.41 MPa	38%	

Doors and windows were constructed of 30×50 mm timber section with a bearing of 75 mm on the wall. The floor was constructed of 10 mm thick and 85 mm wide "Rimu" tongue-and-groove flooring nailed to 35×125 mm timber joists. The joists were nailed to 35×50 mm wooden wall plates laid on the front and back walls. The wall plates just rested on the wall without any mechanical anchorage with the wall. The end joists were nailed to the side walls, and were structurally isolated from the floor planks to isolate these side walls from the front and back walls. A tiled roof was laid on a 33-degree pitched timber frame and accommodated around 2 t of the additional mass. Roof purlins were simply seated on the gable walls without any nailing. To observe the relative performance of different roofing practices, all roof tiles on one pitch and alternate roof tiles on the other pitch were tied down with binding wires to the purlins when the model was tested in the longitudinal direction. However, when the model was tested in the transverse direction, half of the tiles on one side were untied, while the rest were alternatively tied down; and on the other slope all the tiles were tied down.

2. Experimental Procedure

A total of 61 and 41 channels of instruments were employed to collect data during the dynamic excitations of the model in the longitudinal and transverse directions, respectively. Accelerometers and linear potentiometers were the principal instruments used. The potentiometers were employed to measure (i) the crack openings at pre-determined locations, (ii) shear deformations of the piers, and (iii) sliding between floor/roof and the walls. In order to measure the relative displacement between floor/roof and face-loaded walls, potentiometers were attached at the floor and roof levels along the central line of the side solid wall during the longitudinal shakings and to the front wall during the transverse shakings. Moreover, the in-plane shear deformations of the piers were measured by attaching potentiometers diagonally across the piers 1–4 in the front wall (see Figure 2) during the longitudinal shakings and across the piers 11–14 (see Figure 2) during the transverse shakings. Similarly, one accelerometer was attached to the base slab to track the input acceleration history, and accelerometers were attached to the middle of the four walls at the floor and roof levels to measure movement of the model (at different locations) in the direction of shaking. Data was collected via a purpose-built data acquisition system operating at 400 and 1000 Hz during the longitudinal and transverse shakings, respectively.

The testing program was basically divided into two parts: (i) identification of dynamic characteristics; and (ii) investigation of the behaviour of the building model during the strong shaking. For the identification of dynamic properties, white-noise shaking tests were conducted. To investigate the building response to strong shaking, the model was subjected to frequency-scaled earthquake ground motions. The sequence of the shaking table tests performed in the longitudinal and transverse directions is presented in Tables 2 and 3, respectively.

3. Experimental Results

3.1 Longitudinal Direction Shaking

Cracks developed during different stages of the longitudinal shaking are shown in Figure 2. Figure 3 presents the photographs of the damage suffered by the model during this shaking. It should be noted that no instability of any part of the model was observed (excluding gable walls) during the longitudinal shaking tests. A vertical crack was observed in the mortar joint of the rowlock brick just above the front wall door after the Taft (0.2*g*) excitation as shown in Figure 2. During the Taft (0.3*g*) excitation, one of

the gable walls cracked and started to rock at the eaves level, just below the additional-load-fixing level of the end wall. A residual displacement of 3 mm was observed at the top of the gable wall at the end of this excitation.

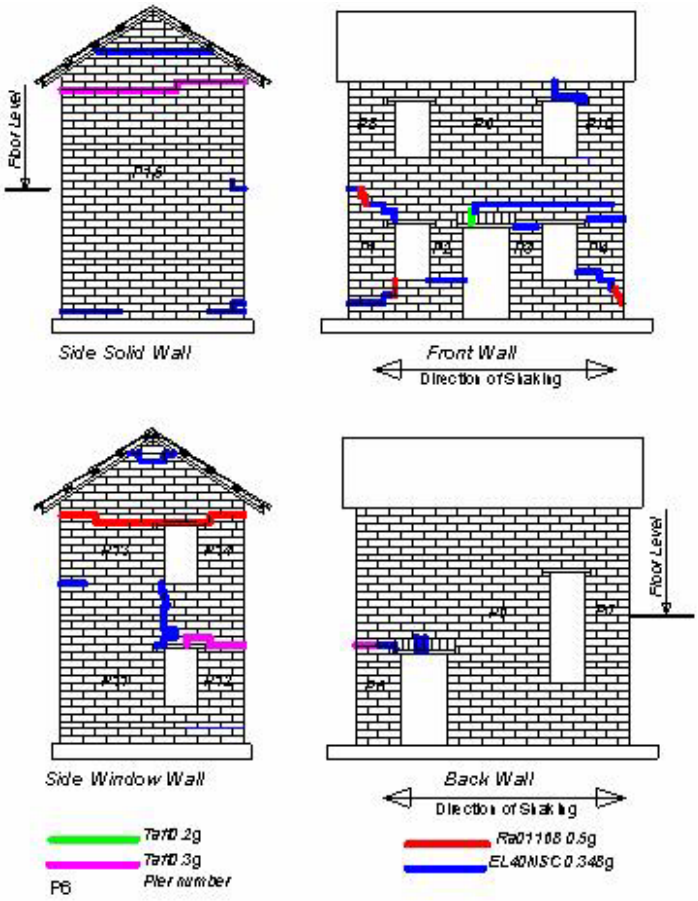

Fig. 2 Crack propagation patterns and their locations (in longitudinal direction)

Table 2: Longitudinal Shaking Test Sequence

S. No.	Acceleration Record	PGA (*g*)	Code	Purpose
1	White Noise	0.02	Wn (0.02*g*)	Study of Dynamic Characteristics
2	White Noise	0.05	Wn (0.05*g*)	Study of Dynamic Characteristics
3	Taft2721	0.2	Taft (0.2*g*)	Moderate Level Earthquake
4	Taft2721	0.3	Taft (0.3*g*)	Moderate Level Earthquake
5	Umbria March (RA01168 551)	0.5	Ra01168 551 (0.5*g*)	Severe Earthquake
6	El Centro	0.348	EL40NSC	Moderate-to-Severe Earthquake

Table 3: Transverse Shaking Test Sequence

S. No.	Acceleration Record	PGA (*g*)	Code	Purpose
1	White Noise	0.05	Wn (0.05*g*)	Study of Dynamic Characteristics
2	Taft2721	0.2	Taft (0.2*g*)	Moderate Level Earthquake
3	White Noise	0.05	Wn (0.05*g*)	Study of Dynamic Characteristics
4	Taft2721	0.3	Taft (0.3*g*)	Moderate Level Earthquake
5	White Noise	0.05	Wn (0.05*g*)	Study of Dynamic Characteristics
6	White Noise	0.05	Wn (0.05*g*)	Study of Dynamic Characteristics
7	El Centro	0.348	EL40NSC	Moderate Level Earthquake
8	White Noise	0.05	Wn (0.05*g*)	Study of Dynamic Characteristics

9	Umbria March (RA01168 551)	0.5	Ra01168 551 (0.5*g*)	Severe Earthquake
10	Umbria March (RA01168 551)	0.7	Ra01168 551 (0.7*g*)	Severe Earthquake
11	White Noise	0.05	Wn (0.05*g*)	Study of Dynamic Characteristics
12	Northridge	0.8	Sylm949	Strong Earthquake
13	Nahanni	0.8	Nahanni	Strong Earthquake
14	White Noise	0.05	Wn (0.05*g*)	Study of Dynamic Characteristics

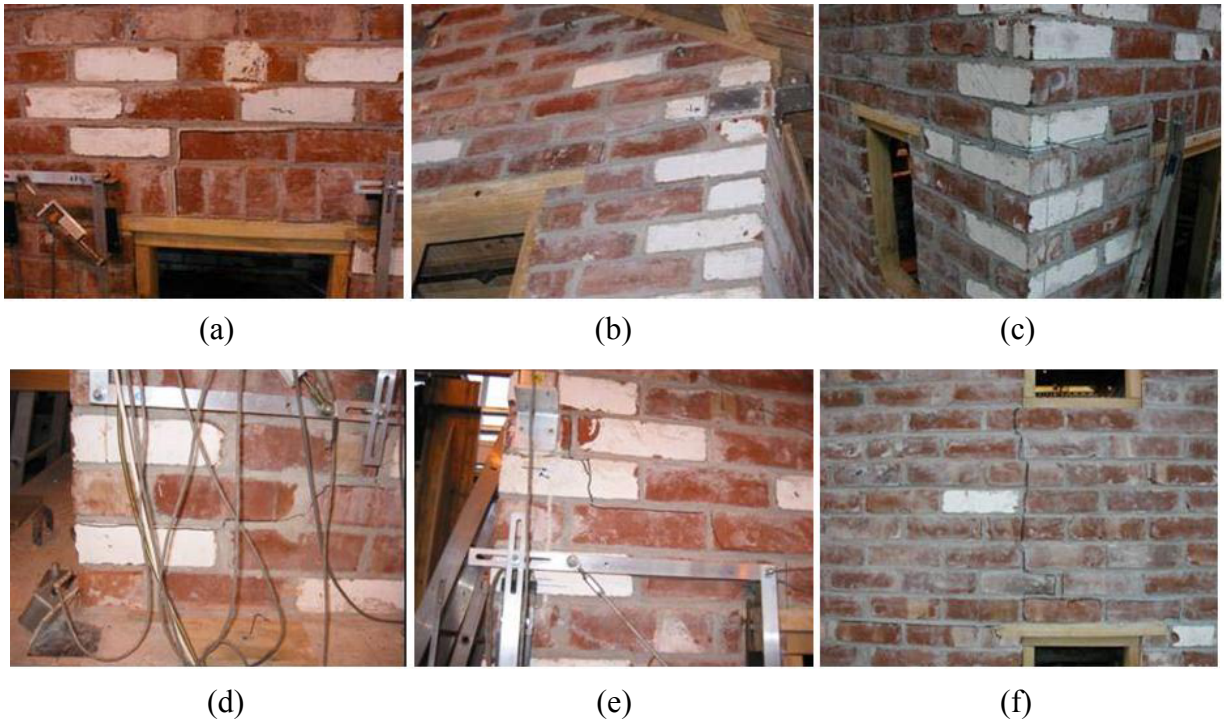

(a) (b) (c)

(d) (e) (f)

Fig. 3 Visually observed damage during the excitation (in the longitudinal direction): (a) horizontal and rowlock brick joint cracking; (b) cracking at the base of gable wall; (c) cracking at the top of pier; (d) stair-step cracking at the bottom of pier; (e) stair-step cracking at the top of pier; (f) vertical and horizontal cracking in side-window wall

During the Ra01168 551 (0.5*g*) excitation, the other gable wall also cracked at its base (as seen in Figures 2 and 3(b)) and started to rock. A few more cracks were observed just below the top of the gable walls, and in the bottom and top of the front-wall piers (as shown in Figure 3(c)). A compression crack below the pier 4 at the wall corner and compression edge failure at the bottom of the rocking gable wall and its base were also observed during the subsequent shakings.

As can be seen in Figure 2, a vertical flexural crack developed between the 1st and 2nd storey windows on one side during the EL40NSC excitation. As shown in Figures 3(d) and 3(e), the cracks developed just below and above the pier in the earlier shakings articulated into a stair-stepped crack pattern. A horizontal crack was also observed just above the floor-wall plate in the front wall. From the maximum displacements measured during different shakings, the weighted displacements are calculated at the seismic centre of mass of the model and are listed in Table 4 for both longitudinal and transverse shaking directions.

3.2 Transverse Direction Shaking

Figure 4 presents the cracks developed, and Figure 5 presents the photographs of damage suffered by the model during different excitations in the transverse direction. It should be noted that no instability of any part of the model (though front and back walls suffered partial instability) was observed during the transverse shaking tests. As can be observed in Figure 4, most of the cracks were concentrated in the out-of-plane wall of the second storey, whereas the (in-plane) side-window wall suffered extensive damage in

both first and second storeys. Cracking was also observed in the solid side wall. Most of the cracks developed during earlier excitations in the longitudinal direction widened and extended during the stronger excitations of this phase of testing.

Table 4: Maximum Displacements at the Seismic Mass Centre and Measured Hysteretic Damping

Shaking Direction	Excitation	Maximum Displacement (mm)	Measured Hysteretic Damping (%)
Longitudinal	Taft (0.2*g*)	0.98	9.1
	Taft (0.3*g*)	0.82	7.3
	Ra01168 551 (0.5*g*)	3.9	31.5
	EL40NSC	2.36	18.5
Transverse	Taft (0.2*g*)	2.58	15.9
	Taft (0.3*g*)	3.74	22.6
	EL40NSC	4.65	21.5
	Ra01168 551 (0.5*g*)	6.85	39.4
	Ra01168 551 (0.7*g*)	10.07	41.9
	Sylm949	11.1	52.3
	Nahanni	15.33	30.3

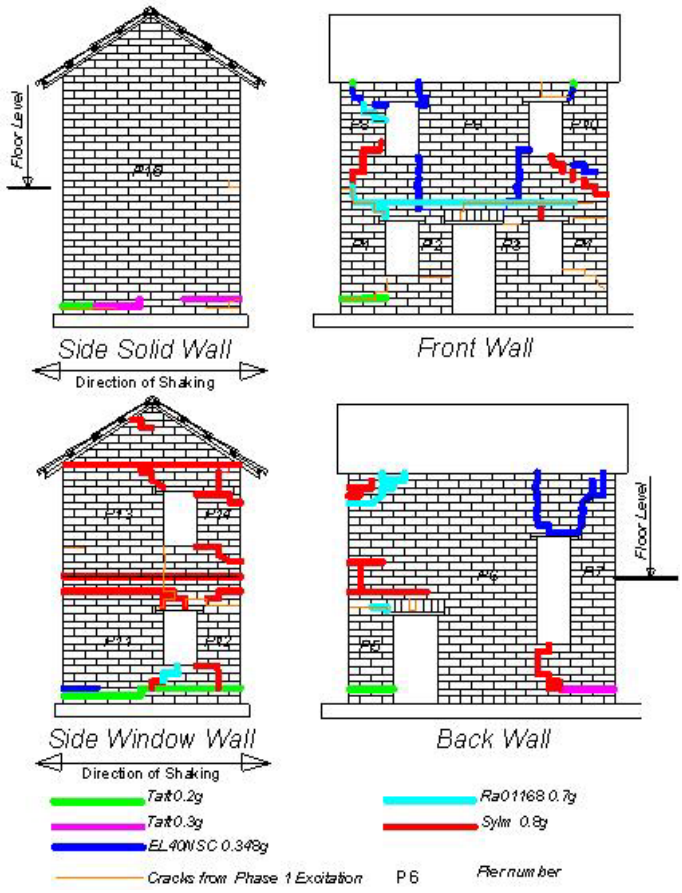

Fig. 4 Crack propagation patterns and their locations (in transverse direction)

Small vertical cracks were observed above the second-storey windows of the front wall after the Taft (0.2*g*) excitation. During the Taft (0.3*g*) excitation, a few new cracks opened at the bottom of the side walls. During the EL40NSC excitation, extensive cracks developed in the out-of-plane walls as seen in Figure 4. Vertical cracks developed along the line of jambs of the second storey openings in the front wall, practically isolating the wall from the in-plane walls. Similar vertical or stair-step cracks developed above the long window of the back wall (see Figure 5(d)). Once the severe cracking of the model started, dislocation of the lintel timber pieces and permanent distortion of the opening frames were also observed.

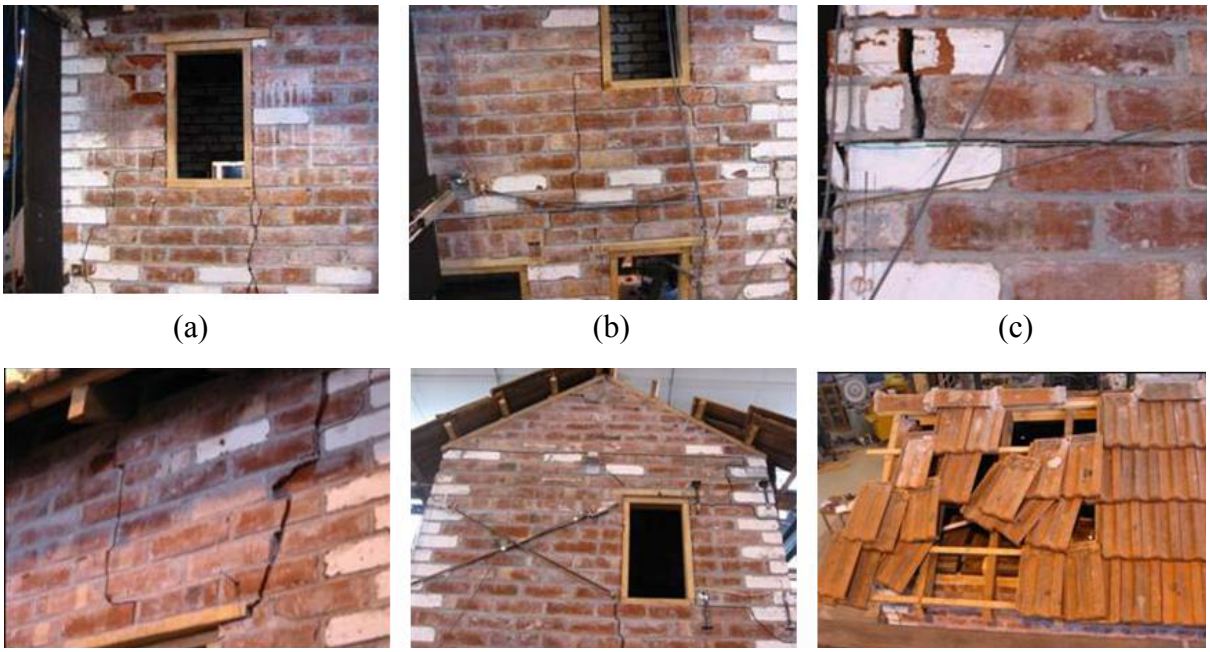

(a) (b) (c)

(d) (e) (f)

Fig. 5 Visually observed damage during the excitation (in the transverse direction): (a) vertical and stair-step cracking in the front wall; (b) propagation of cracks through and along the spandrel beam; (c) cracking at the floor level in the side-window wall; (d) cracking in the back wall just above the long window; (e) cracking at the bottom of gable wall and around windows (note also the diagonal instruments used for inferring shear strains, while the vertical ones in the right-hand pier are for inferring rocking effects); (f) scattering and falling of tiles (note that the tied-up tiles did not slide)

During the Ra01168 551 (0.7*g*) excitation, cracks that had previously developed widened, and some new cracks developed. A stair-step crack was observed just above the first-storey window and in the pier of the second-storey wall (see Figure 5(a)) in the front wall. The front wall rocked about a horizontal crack along the mortar bed joint that was observed at the floor level during this shaking. During the Sylm949 excitation, extensive cracks developed in both in-plane and out-of-plane walls. As can be seen in Figures 4 and 5(b), more stair-step cracks were observed in the spandrel beam of the front wall and along the mortar bed joint in the back wall. Also what can be clearly seen in Figure 4 is a full-length horizontal crack developed along the bottom of the gable wall of the side window-wall. Similar crack was also observed at the floor level of the side window-wall. The vertical cracks in the spandrel beam and below the first-storey window of the side window-wall effectively divided the wall in two significantly tall piers. During the Nahanni excitation, the cracks further widened; however, no new cracks were observed.

No significant relative displacement between the floor and the supporting walls was observed. This contradicts the observed behaviour during past earthquakes where relative movement between the floor structure and walls was reported (Bruneau, 1994; NSET-DEQ, 2000). The first reason could be that the model was quite stable until the end of the testing without much distress in the first storey. The other reason could be that there was around 2 t of mass on the floor structure that mobilized friction between the floor wall plate and the supporting walls; the friction would not exist in this magnitude in a real structure.

It is noteworthy that some of the roof tiles, which were not tied down with the roof structure, scattered badly and that a few of them slid off the roof slope during the RA01168 551 (0.5*g*) excitation. As shown in Figure 5(f), these tiles slid off catastrophically during the RA01168 551 (0.7*g*) excitation and other big excitations. It is interesting to note that the tile sliding started from the roof edge. However, no tiles tied down with the timber frame moved much and slid off the roof. It may be noted that the model survived higher accelerations than those expected for the real URM masonry buildings in the field, mainly because no local failure that would lead to instability started and thus the building behaved like a box.

This can be attributed to good connection between the orthogonal walls at the junctions, good connection between the floor/roof and walls, diaphragm effect, better construction/material quality, and to good foundation which is usually not available in most real buildings.

3.3 Frequency Domain Observations

Dynamic properties of the model were computed from the response acceleration time histories collected during the shaking table test. To avoid the effect of input amplitude, transfer functions for the individual channels were calculated by normalizing the Fast Fourier Transform (FFT) of each channel response by the FFT of the input motion (which, in this case, is the input acceleration at the base slab level). Intrinsic damping was calculated from the transfer function plots by applying the half-power bandwidth method (Chopra, 1995). The mode shapes were calculated by taking ratios of the peaks in the transfer functions for different degrees of freedom at any particular natural frequency. As the constant of proportionality is same for all degrees of freedom for any particular mode, the ratios of peaks in the transfer functions for different degrees of freedom at that natural frequency are equal to the ratios of the mode shapes for that mode (Bracci et al., 1992). The dynamic stiffness of the model was estimated by using the relation $K = 4\pi^2 Mf^2$, where only the first mode was considered. In this relation, M denotes the seismic mass of the building and f the measured frequency in Hz.

3.4 Inferred Hysteretic Damping

The total equivalent viscous damping in a dynamic inelastic system is a sum of hysteretic damping, radiation damping associated with the rocking, and intrinsic damping due to internal interactions within the system. From the "displacement versus acceleration" hysteretic loops, the hysteretic damping can be estimated by using $\varsigma_{\text{eq}} = E_D / 4\pi E_{so}$ (Chopra, 1995), in which E_D denotes the total area enclosed by the hysteretic loop and E_{so} the strain energy imposed on the system.

From the displacement-acceleration plots of different sets of channels, hysteretic loops for the same time intervals were developed. For these loops, hysteretic damping was estimated and then weighted for their tributary mass. Similarly, the corresponding displacement of the seismic mass centre was estimated for these loops. The equivalent hysteretic damping after each series of shaking (i.e., calculated from the recorded hysteresis loops) is listed in Table 4.

ANALYTICAL STUDY

An analytical investigation of the model was conducted through finite element simulation and simple rational calculations. The calculations based on a plastic mechanism analysis were performed to estimate the strength of the model. The dynamic structural characteristics of the models were assessed through finite element simulation and a static condensation technique. It may be noted that although it was intended to construct a flexible diaphragm, the resulting floor was rigid because of the tongue and groove flooring, high strength/stiffness of the diaphragm, scale effect, connection between the wall and floor, etc. Hence, a rigid diaphragm system was assumed wherever it was needed in the analytical modelling.

1. Finite Element Analysis

A linear elastic finite element model using four-node shell elements for walls was developed in SAP2000 (CSI, 2002). Masonry was assumed to be isotropic (Dhanasekar et al., 1982). The floor joists of the model comprised beam elements pinned at the ends. The floor boards were modelled as discrete plane elements isolated from the walls. Roof rafters and ties were discretised as beam elements, and ties were pinned at the ends. The dynamic modulus of elasticity was assumed as 390 MPa, based on the average measured crushing strength of masonry (Mengi and McNiven, 1986), rather than the measured static modulus of 6100 MPa. It is because the dynamic modulus of elasticity is much lower than the static one (Mengi and McNiven, 1986). This point is also proved by the measured frequencies. If the static modulus of elasticity had been used to calculate the frequency in the longitudinal direction, the predicted frequency of the model would have been around 40 Hz, which is far greater than the measured values.

The static analysis of the model suggested flexural cracking to be the dominant mode of damage. In longitudinal shakings, analyses showed that the cracks would develop at the top and bottom of the front-wall piers. In transverse shakings, flexural cracks were expected to develop in the front wall above the

second-storey windows corners. With increasing levels of lateral loads, the in-plane walls showed development of tensile cracks at the bottom. The estimated base shear capacity, at which the cracks would develop during the longitudinal and transverse shakings, and the corresponding deflections are shown in Table 5.

Table 5: Estimated Lateral Load Coefficient for the Initiation of Cracking and Corresponding Deflections

Loading Direction	Base Shear Coefficient at the Crack Initiation	Deflections (mm)								Remarks
		In-plane Wall-1		In-plane Wall-2		Out-of-Plane-1		Displacement of the Seismic Mass		
		1st Floor	Eaves Level	1st Floor	Eaves Level	1st Floor	Eaves Level	1st Floor	Eaves Level	
Longitudinal	0.36	0.89	1.3	1.03	1.63	0.92	1.49	0.94	1.47	Controlled by the In-plane Cracking
Transverse	0.30	0.77	1.6	0.65	1.45	0.8	1.99	0.79	1.85	Controlled by the Out-of-Plane Cracking

Table 6 presents the frequencies computed from the dynamic analysis by using the linear finite element model. The out-of-plane behaviour of the walls normal to the shaking was observed as the most dominant mode of vibration. For comparison, the frequency and mode shapes of the model were also estimated by assuming a undamped two-degrees-of-freedom system and by using a static condensation technique (Chopra, 1995). For the calculation of frequency, mass is assumed to be lumped only at the floor and roof levels. In full-scale URM houses, these types of floors hardly contribute 10-20% of the building mass, and such houses are better represented by a distributed-mass system. However, in the tested model, additional mass for the stress simulation (which was around 50% of the model mass required) was fixed to the floor and roof, thereby justifying the lumped mass assumption. The finite element analysis in SAP2000 also lumps the mass at certain levels, even if the system is a distributed-mass system. A comparison of the dynamic properties from the finite element analysis and from the static condensation technique is shown in Table 6.

Table 6: Dynamic Characteristics of the Model

Shaking Direction	Method of Analysis	Frequencies (Hz)		Mode Shapes	
		Analytical	Experimental	Analytical	Experimental
Longitudinal	Static Condensation	$\begin{Bmatrix}10\\28\end{Bmatrix}$	(11.7)	$\begin{Bmatrix}1.0 & -0.77\\0.72 & 1.0\end{Bmatrix}$	$\begin{Bmatrix}1\\0.81\end{Bmatrix}$
	FEM-SAP2000	(8.7)			
Transverse	Static Condensation	$\begin{Bmatrix}9.3\\21.7\end{Bmatrix}$	(9.8)	$\begin{Bmatrix}1.0 & -0.72\\0.55 & 1.0\end{Bmatrix}$	$\begin{Bmatrix}1\\0.49\end{Bmatrix}$
	FEM-SAP2000	(7.5)			

2. Mechanism Analysis

Base shear capacity is the capacity of the building at which the building gets to the onset of plastic behaviour. Thus the base shear capacity/coefficient of the model is calculated in this study from the mechanism analysis as prescribed by the NZSEE guidelines. A force-based approach (Paulay and Priestley, 1992) is used to determine the in-plane strength of the model. Overturning moments were considered for strength estimation of the wall piers. For the estimation of base shear coefficients at cracking, a storey-failure mechanism of the model structure (involving pier action of the wall) was assumed. To assess the strength of the model, plastic analysis was conducted. The front wall (with door and window openings) was found to be dominated by rocking, whereas the back wall was found to be shear-dominated in the longitudinal shaking.

For the front wall, it was predicted that cracking would initiate at a base shear of 24 kN and a rocking mechanism would develop at 32 kN. The model was expected to develop into a mechanism at a base shear coefficient of 0.7, i.e., at the base shear of 54 kN. The side walls were predicted to develop tensile cracks at their bases in transverse shaking at a base shear coefficient of 0.36, i.e., at the base shear of 28 kN. After that, it was obvious that these walls would globally rock about their bases. The model was expected to rock at a global base shear coefficient of 0.55, i.e., at the global base shear of 42 kN.

3. Comparison of Experimental and Analytical Results

As predicted analytically, the front-wall ground-floor piers rocked when the model was shaken in the longitudinal direction. However, the rocking surfaces manifested in stair-step cracking as well in a few piers rather than just at the bottom or at the top. As predicted, the back wall turned out to be much stronger than the front wall and did not suffer any damage in general. The experimental pier cracking strength in longitudinal shaking was 23% higher than the analytical prediction. However, at the first cracking, 0.69 mm displacement was observed as compared to 0.18 mm at the eaves level calculated analytically by using the static modulus of elasticity. This shows that the model was much more flexible than that estimated by using the static modulus of elasticity.

In the transverse direction, the predicted cracking strength was found to be 17% higher than the experimentally observed strength. However, once the model started global rocking, the predicted base shear coefficient was found closer to the observed one. Some cracks observed during the experiments were found in reasonably good agreement with the predictions of the static analysis. Differences between the experimental and analytical predictions of elastic frequency and deflection were considerable if estimated using the static modulus of elasticity. For example, the experimental fundamental frequency in the longitudinal direction observed before the cracking was 13.7 Hz, as against 33.1 Hz and 38 Hz estimated respectively from SAP2000, and static condensation by using the static modulus of elasticity. On the other hand, using the value of dynamic modulus of elasticity estimated using the crushing strength of masonry (Mengi and McNiven, 1986) was reasonable for the frequency prediction. This was not the case however with the deflection prediction. Other sources of error in the estimation of frequency and displacements could be the uncertainty associated with the load transfer mechanism, flange effect, and with the assumed material properties.

DEVELOPMENT OF RESPONSE AND FRAGILITY FUNCTIONS

In order to conduct seismic risk analysis, probabilistic relationships between the seismic intensity of the earthquakes and the maximum response (called the response function), and between the maximum response and a damage measure (called the fragility function) need to be established. If the earthquake intensity is expressed in terms of PGA (which is not uncommon in seismic risk assessment methodologies), the results of the different series of the shaking table tests will give a series of PGA versus maximum response points. As the number of data points is limited by the number of tests and the maximum response during the later tests will be influenced by the prior shakings, an alternate method to predict the PGA versus the maximum response is implemented here. As derived by Pekcan et al. (1999), the relationship between the earthquake intensity (i.e., PGA) and the maximum displacement of a structure can be expressed as higher of

$$\mathrm{PGA} = 2\pi \sqrt{\frac{C_c \Delta_{\mathrm{Prototype}}}{g}} B_\varsigma \tag{1a}$$

and

$$\mathrm{PGA} = 0.4 C_C B_\zeta \tag{1b}$$

where C_c is the base shear capacity as determined from the finite element analysis (= 0.7 for the longitudinal direction and 0.55 for the transverse direction), $\Delta_{\mathrm{Prototype}}$ is the maximum displacement of the seismic mass center of the prototype, and B_ζ is a damping related reduction factor. According to Martinez (2002), this factor is given by

$$B_{\varsigma} = \sqrt{\frac{0.05 + \varsigma_{\text{eff}}}{0.1}} \tag{2}$$

where ς_{eff} is the effective viscous damping estimated from the displacement-damping relationship as (Pekcan et al., 1999)

$$\varsigma_{\text{eff}} = 0.05 + \frac{2}{\pi}\eta\left(1 - \frac{\Delta_y}{\Delta_{\max}}\right) \tag{3}$$

In Equation (3), η is the efficiency factor taken as 0.5, Δ_y is the displacement at the first crack (as obtained from the test results; it is equal to 0.7 and 1.05 mm for the longitudinal and transverse directions, respectively), and $\Delta_{\max}$ is the maximum displacement at the seismic mass centre. The effective viscous damping predicted by Equation (3) includes the inherent damping in the system (assumed as 5%) and the hysteretic damping estimated as $2\eta/\pi\left(1-\Delta_y/\Delta_{\max}\right)$. For verification, the equivalent hysteretic damping in the longitudinal and transverse directions predicted by this expression is plotted in Figure 6 together with the hysteretic damping estimated from the experimental results. It can be seen in the figure that Equation (3) captures the variation of damping with the displacement amplitude reasonably well. Now, using this damping and the base shear coefficient determined earlier, a deterministic median response function can be established by using Equation (1). The incorporation of uncertainties in the response function is described later.

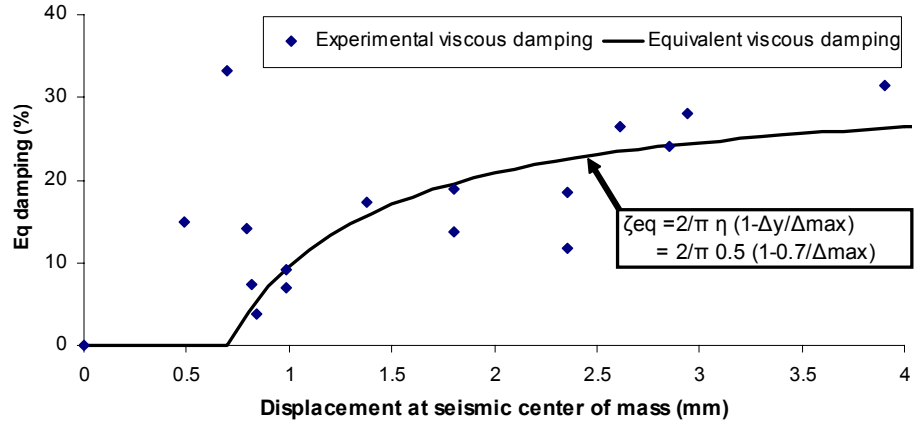

(a)

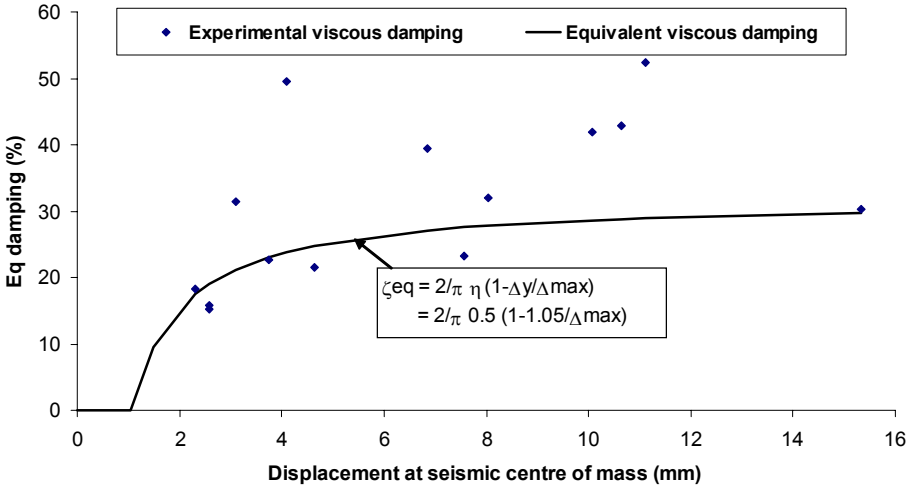

(b)

Fig. 6 Theoretical prediction and experimental verification of displacement versus equivalent viscous damping curve in the (a) longitudinal, and (b) transverse directions

To generate fragility functions, numbers from 1 to 5 (that refer to increasing level of damage) are used as defined in Table 7. This is a common form of damage classification format and has been adopted by NIBS (1999). Based on post-earthquake utility and life-safety considerations, the drift ratios observed during the tests at the onset of different levels of damage are summarized in Table 8. It may be noted that the damage state versus drift relationships are assumed to be deterministic in this study and due to lack of data, uncertainties in these fragility relationships (which are inevitable) are not considered. Next, on combining the response and fragility functions, the median PGAs corresponding to the boundaries of different damage states are calculated using Equations (1)–(3) and the results are presented in Table 8.

Table 7: HAZUS Classification of Damage States Following an Earthquake (NIBS, 1999)

Damage State	Damage Descriptor	Post-Earthquake Utility of Structure
1	None (pre-yield)	Normal
2	Minor/Slight	Slight Damage
3	Moderate	Repairable Damage
4	Major/Extensive	Irreparable Damage
5	Complete Collapse	

Table 8: Damage State Classification

Damage State	Drift Limit (%)	$\Delta_{experimental}$ (mm)	ς_{eff} (%)	B_{ς}	$\Delta_{Prototype}$ (mm)	Expected PGA	Post-Earthquake Utility
1							No Damage
	0.1	2	20.1	1.58	4	0.35	
2							Slight Damage
	0.5	10	33.5	1.96	20	0.43	
3							Repairable Damage
	0.9	18	35.0	2.00	36	0.56	
4							Irreparable Damage
	1.3	26	35.5	2.01	52	0.68	
5							Complete Collapse

In dynamic analysis, the resulting variability in the response function results entirely from the randomness of the input motion, i.e., if two different records are scaled to the same PGA, the maximum response would still be different. As the computational modeling is conducted using crisp input data, the epistemic uncertainty is not accounted for. However, the structural resistance, both in terms of strength and displacement capacities, is also inherently variable. To encompass the randomness of seismic demand along with the inherent randomness of the structural capacity and the uncertainty due to the inexactness of the computational modeling, an integrated approach as suggested by Kennedy et al. (1980) is used in this study. If the randomness and uncertainties are assumed to be distributed normally or log-normally (which is a common assumption in probabilistic seismic risk assessment), the composite value of the lognormal coefficient of variation (i.e., the dispersion factor) can be expressed as

$$\beta_{C/D} = \sqrt{\beta_C^2 + \beta_D^2 + \beta_U^2} \tag{4}$$

in which β_C (assumed to be 0.2 in this study) is the coefficient of variation for the capacity that arises as a result of the randomness in the material properties that affect strength; β_D (assumed to be 0.52 in this study) is the coefficient of variation for the seismic demand that arises from the record-to-record randomness in the earthquake ground motion suite; and β_U is the lognormal dispersion parameter for the modelling uncertainty (this is found to be approximately equal to 0.2 based on the results given in Table 4). On using the aforementioned values of β_C, β_D, β_U, Equation (4) gives $\beta_{C/D}$ = 0.6.

As indicated earlier, the PGAs shown in Table 8 are the median (or 50th percentile) values. Using these median values and the lognormal coefficient of variation of 0.6 (as calculated above), the probability of the damage during an earthquake ground motion (of a given PGA) being within a given state can be shown graphically through vulnerability curves as in Figure 7. Two vertical lines are drawn at 0.4*g* and 0.72*g* to represent, respectively, the design basis earthquake (DBE) and the maximum considered earthquake (MCE) at Wellington, while following the seismic hazard reported in the New Zealand loading standard NZS1170.5 (NZS, 2004). The intersection of these vertical lines with the damage probability curves gives the probabilities of different damage states for the corresponding seismic hazard. Figure 7 shows that about 30% of the URM houses will suffer irreparable damage (i.e., DS4) or collapse (i.e., DS5) during a DBE, while up to 70% may suffer damage that would be either slight or repairable (i.e., DS1–DS3). However if an MCE was to strike, then about 65% of such houses might suffer irreparable damage or collapse, with the remaining 35% suffering minor or repairable damage.

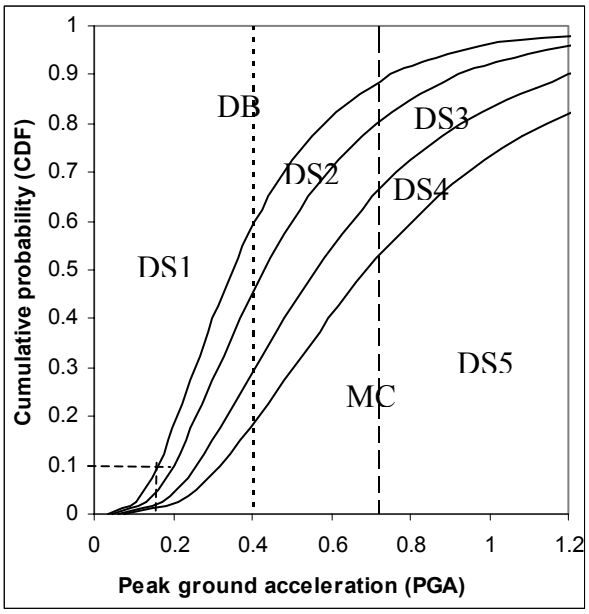

Fig. 7 Vulnerability curves related to the HAZUS damage states

FINANCIAL SEISMIC RISK ASSESSMENT FRAMEWORK

Communicating seismic risk to decision makers is an important aspect of performance-based earthquake engineering (PBEE). One such communication tool is the expected annual loss (EAL), which can be expressed in a dollar value. EAL incorporates the entire range of seismic scenarios, return rates, and expected damages into a median loss value in dollars. Though there are many methods of quantifying financial risk, EAL is especially useful to decision makers for a cost-benefit analysis of design alternatives for new structures, or for evaluating seismic retrofit alternatives for existing structures. Moreover, EAL can be easily accounted for by including it in the operating budgets.

In addition to the response and fragility functions, an EAL assessment process also requires a seismic hazard occurrence relationship (correlating earthquake intensity with its annual frequency of occurrence) and a loss model (correlating damage with the probable loss). When these four relationships are combined using a quadruple integral shown below, seismic risk can be quantified in terms of EAL as (Dhakal and Mander, 2005)

$$\mathrm{EAL} = \int_0^1 \int_0^1 \int_0^1 \int_0^1 L_R \left| \mathrm{d}P\left[L_R \mid \mathrm{DM}\right] \right| \left| \mathrm{d}P\left[\mathrm{DM} \mid \mathrm{EDP}\right] \right| \left| \mathrm{d}P\left[\mathrm{EDP} \mid \mathrm{IM}\right] \right| \left| \mathrm{d}f_a\left[\mathrm{IM}\right] \right| \tag{5}$$

In Equation (5), IM is the intensity mesure; f_a [IM] is the annual frequency of an earthquake of a given intensity IM; EDP is the engineering demand parameter; DM is the damage measure; L_R is the loss ratio (i.e., decision variable); $P[A \mid B]$ is the shortened form of $P[A \geq a \mid B = b]$; and $\mathrm{d}P[A \mid B]$ is the derivative of the conditional probability $P[A \mid B]$ with respect to A. In this study, rather than using Equation (5)

analytically, the integrations are carried out numerically. In fact, the integrations of the response function (over *P*[EDP | IM] by using the IM versus EDP relationship) and the fragility function (over *P*[EDP | IM] by using the EDP versus DM relationship) have been implicitly performed in a deterministic manner (for median values) in Table 8. Thus, on using the combined uncertainty predicted by Equation (4), probabilistic vulnerability curves (i.e., IM versus DM curves) have been generated in Figure 7, which can be used for integration over *P*[DM | IM]. A hazard recurrence relationship (between f_a and IM, for the integration over f_a [IM]) and a loss model (between DM and L_R, for the integration over $P[L_R \mid \text{DM}]$) are now established to complete the remainder of the EAL assessment process, as explained below.

ASSESSMENT OF HAZARD SURVIVAL PROBABILITY

1. Earthquake Recurrence Relationship

Based on historical earthquake data, relationship between the peak ground acceleration (*PGA*) of earthquakes (denoted as a_g) with their annual frequency of occurrence (f_a) has been established as:

$$a_g = \frac{a_g^{\text{DBE}}}{(475 f_a)^q} \tag{6}$$

where a_g^{DBE} is the PGA for the DBE (with 10% probability of occurrence in 50 years), and q is an empirical constant found to be equal to 0.33 for seismic hazard in New Zealand (NZS, 2004).

2. Hazard Survival Curves

Vulnerability curves of Figure 7 can now be re-plotted by changing the horizontal axis from IM to f_a and by using the earthquake recurrence relationship established earlier. Such curves are called hazard survival curves, which show the annual probabilities of the seismic damage exceeding different limit states. Figure 8 shows the hazard survival curves for a typical URM house, which also give the probability of damage in such URM masonry houses falling within a limit state when an earthquake of a given annual frequency strikes. Two vertical lines representing the annual probabilities of DBE ($f_a \sim 0.002$) and MCE ($f_a \sim 0.0004$) are also shown in the plots for reference. The intersections of any vertical line through a value of f_a with the hazard survival curves give the probabilities of these damage states not being exceeded during the earthquakes of that annual probability of occurrence. The thus-obtained survival probabilities of different damage states during the earthquakes of different frequencies are shown in Table 9 for a typical URM house of the tested type. Similarly, Table 10 shows the probabilities of being in a given damage state (i.e., confidence intervals) for a typical URM house. For example, the second row in Table 9 implies that if an earthquake of annual frequency of 0.01 (i.e., with the return period of 100 years) strikes, the probability of DS1 not being exceeded in a URM house of the tested category is 74%; and the corresponding probabilities for the damage states DS2, DS3 and DS4 are 84%, 92% and 96%, respectively. Similarly, the second row of Table 10 indicates that during a 100-year return period earthquake, there is a 74% chance that the damage state of a URM house will be DS1, 10% chance that the damage will be in the range of DS2, 8% chance that the damage will be in DS3, 4% chance that the damage will be in DS4, and 4% chance that the damage state will be DS5.

FINANCIAL IMPLICATIONS OF EARTHQUAKES

1. Loss Model

To quantify financial loss, a loss model must be established to relate damage measure (DM) to the dollar value. In this study, the financial implication of each damage state is represented by a 'loss ratio' (L_R), which is the ratio of the cost necessary to restore the structure to full working order to the replacement cost. Deciding the cost implication of each damage state is a subjective process, and the accuracy of the decided value will depend largely on the amount of time devoted to researching the repair costs and their variations by the extent of damage, location of building, etc.

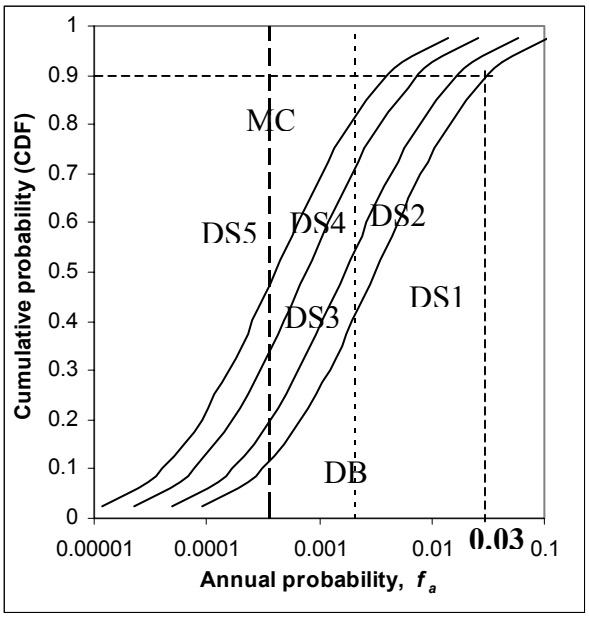

Fig. 8 Hazard survival curves related to the HAZUS damage states

Table 9: Probability *P*[DS ≤ DS*i*] of Not Exceeding a Given Damage State of an URM House

f_a	$i = 1$	$i = 2$	$i = 3$	$i = 4$	$i = 5$
0.1	0.97	1	1	1	1
0.01	0.74	0.84	0.92	0.96	1
0.001	0.26	0.39	0.56	0.69	1
0.0001	0.03	0.06	0.12	0.22	1
0.00001	0	0	0.02	0.02	1
0.000001	0	0	0	0	1

Table 10: Probability *P*[DS = DS*i*] of Being in a Given Damage State of an URM House

f_a	$i = 1$	$i = 2$	$i = 3$	$i = 4$	$i = 5$
0.1	0.97	0.03	0	0	0
0.01	0.74	0.1	0.08	0.04	0.04
0.001	0.26	0.13	0.17	0.13	0.31
0.0001	0.03	0.03	0.06	0.1	0.78
0.00001	0	0	0.02	0	0.98
0.000001	0	0	0	0	1

The assumed values and the likely ranges of loss ratios for different damage states are shown in Table 11. As no damage or repair is expected in the elastic (damage) state DS1, no financial loss is incurred, and the loss ratio for DS1 is therefore zero. Loss ratio for DS2 is likely to fall between 0.05 and 0.15 to account for minor repairs due to slight but tolerable damage, and L_R is assumed to be 0.1 for DS2. The loss ratio for DS3 may vary from 0.2 to 0.4 for repairing the incurred moderate damage and to restore functionality, and a representative value of 0.3 is adopted in the present analysis. "Irreparable damage" under DS4 demands complete replacement, as repair may be uneconomical; hence the loss ratio of 1 is used here. Similarly for DS5, which refers to complete failure/collapse, the value of loss ratio is 1. It has been shown (Dhakal and Mander, 2005) that financial risk is sensitive to the values of loss ratios, especially for DS2 and DS3. Hence, good judgement should be applied in deciding these values. Also, the L_R values for DS1 (i.e., no damage), DS4 (i.e., irreparable damage) and DS5 (i.e., collapse) are certain, and obviously, there are likely to be uncertainties in the L_R values for DS2 (i.e., slight damage) and DS3 (i.e., moderate damage). This study has not attempted to quantify these uncertainties, and therefore those are not taken into account here.

Table 11: Loss Ratios for Different Damage States

	DS1	DS2	DS3	DS4	DS5
Likely Range	0	0.05–0.15	0.2–0.4	1.0–1.2	1
Assumed L_R Value	0	0.1	0.3	1	1

2. Probable Loss in an Earthquake

Using the assigned loss ratios, the contributions of different damage states to the financial loss can be estimated. Table 12 lists the probable financial losses (as fractions of the total replacement cost) due to different damage states when earthquakes with annual frequencies of 0.1, 0.01, 0.001, 0.0001, and 0.00001 strike. Each value given in Table 12 is the product of the probability of being in a given damage state during the earthquakes of given annual frequency (as obtained from Table 10) and the consequence, i.e., the loss ratio for the corresponding damage state (as obtained from Table 11). A graphical version of Table 12 is shown in Figure 9, which exhibits the contributions of different damage states and the total probable loss in the form of a bar chart.

Table 12: Probable Losses Contributed by Different Damage States

f_a	L_R					
	DS1	**DS2**	**DS3**	**DS4**	**DS5**	**Total**
0.1	0	0.003	0	0	0	0.003
0.01	0	0.01	0.024	0.04	0.04	0.114
0.001	0	0.013	0.051	0.13	0.31	0.504
0.0001	0	0.003	0.018	0.1	0.78	0.901
0.00001	0	0	0.006	0	0.98	0.986
0.000001	0	0	0	0	1	1

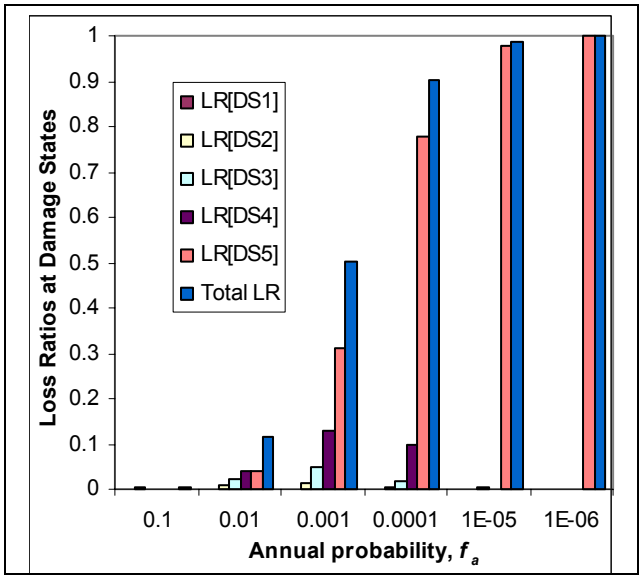

Fig. 9 Deaggregation of losses contributed by different damage states

As expected, DS1 does not incur any financial loss as it does not need any repair. Similarly, the total financial loss incurred by the earthquakes of 0.1 or higher annual frequency is negligible because such frequent events do not inflict any damage requiring repair or replacement (i.e., DS2 or a higher damage state). As the confidence intervals of higher damage states are multiplied by larger values of L_R, the higher damage states contribute more to the probable loss, although the likelihood of the earthquake-induced damage falling into any of these more severe categories is not greater.

The total financial loss due to the earthquakes of a given probability, as shown in the last column of Table 12, is sum of the contributions of the five damage states. The loss hazard curve shown in Figure 10

plots the probable loss of a typical URM house against the annual frequency of exceedance. This curve also gives the information on what would be the financial loss if an earthquake of a given annual frequency strikes once. As expected, larger and rarer the event, greater will be the financial loss. Conversely, for the frequent but low-intensity events, the single-event loss is small.

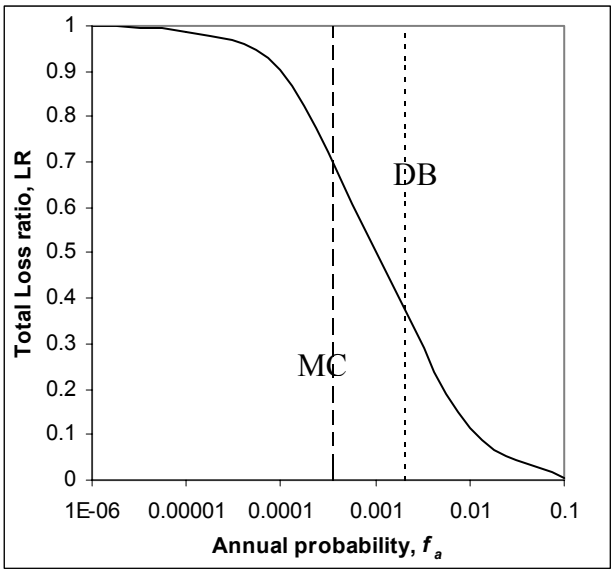

Fig. 10 Loss hazard curve

Two vertical lines corresponding to DBE and MCE are also shown in Figure 10. It is evident that a URM house is likely to lose about 37% and 70% of its value due to the damage incurred by a DBE and an MCE, respectively. A loss of 11% is possible even by the earthquakes of 0.01 annual frequency (i.e., with a return period of 100 years). Similarly, a 50% loss is likely during an earthquake of 1000-year return period.

3. Calculation of Expected Annual Loss (EAL)

The total expected annual loss can be calculated, while using Equation (5), by integrating the loss ratio (L_R) over all possible annual frequencies of the seismic hazard, i.e., between 0 and 1. Thus, it can be expressed in continuous form as

$$\mathrm{EAL} = \int_0^1 L_R \mathrm{d}f_a \tag{7}$$

In discrete form, the expected annual loss (EAL) can be calculated as

$$\mathrm{EAL} = \sum_{\text{all } l_{r,i}} \left(\frac{l_{r,i} + l_{r,i+1}}{2} \right) \left(f_a[L_R = l_{r,i}] - f_a[L_R = l_{r,i+1}] \right) \tag{8}$$

in which $f_a[L_R = l_r]$ is the annual frequency of the loss ratio being equal to a given value l_r, as obtained from the loss hazard curve (see Figure 10). Table 13 shows the annual losses of URM houses. First, the probable loss due to the earthquakes of annual probabilities within a range is calculated, by considering the area subtended by the loss hazard curve (see Figure 10) between two points on the *x*-axis. Then the losses contributed by the earthquakes with different ranges of probabilities are added together to obtain the total expected annual loss (EAL). It may be noted that the annual probability is plotted on logarithmic scale in Figure 10, and that the absolute value of the interval between any two points on the *x*-axis decreases by an order of ten towards the left. Accordingly, the absolute value of the area covered also decreases rapidly in that direction (i.e., in the direction of decreasing probability) in spite of a higher value of the loss ratio.

As can be observed from Table 13, the EAL of typical URM houses is \$8772 for a \$1 million house (i.e., 0.88%). It may be noted that the model considered here overestimates the EAL by overemphasising the contribution of frequent events, which are not likely to cause any significant damage requiring repairs.

This error can be compensated by truncating the data below a certain threshold, which is found by locating the IM at which there will be no damage, say with 90% confidence. As shown in Figures 7 and 8, earthquakes with PGA ≈ 0.16 (i.e., with annual probability of 0.032 and return period of approximately 31 years) will have 90% probability of remaining in DS1 and thus of not inducing any damage to the URM houses. Hence, the contribution to the EAL of earthquakes below this threshold can be excluded for objectivity. In this example, EAL is found to be about 45% lower after truncating the contribution of the earthquakes below this threshold.

Table 13: Annual Financial Risk for Typical URM Houses

f_a	EAL (per $1 million)	
	L_R	ΔEAL
0.1	0.003	
		5265
0.01	0.0114	
		2781
0.001	0.504	
		632
0.0001	0.901	
		85
0.00001	0.986	
		9
0.000001	1	
Total EAL per $1 million		8772

DISCUSSION: IMPLICATIONS FOR OWNERS AND INSURERS

The outcome of this analysis can provide useful information for deciding insurance strategies, but the applicability of any quantitative outcome from this study is limited to the category of URM houses, which are covered by the model used in this study. Any major alterations in the properties of the houses may lead to qualitatively similar but quantitatively different results. Although the tested model was designed to represent URM houses in New Zealand (Bothara, 2004), the population of masonry houses in a country is difficult to be represented by a single type. In New Zealand, masonry houses are not built anymore and there are few existing old masonry houses, which somewhat resemble to the tested house. On the other hand, masonry houses in Nepal (and India) vary widely. Obviously, the outcome of this study is not quantitatively extendable to the URM houses of significantly different features. Nevertheless, the financial risk assessment procedure followed here is applicable to all structural types and by using appropriate fragility and response functions, the expected annual loss for any other type of URM houses can be derived.

The vertical ordinate of the loss hazard curve (see Figure 10) gives the probable loss (due to structural damage) of a house due to an earthquake of a given annual frequency of occurrence. Hence, these curves also represent the financial risk (excluding the loss of contents) to the owners of such houses. Evidently, the smaller and more frequent events will cause only a small loss to the owners of such URM houses. Consequently, owners may be prepared to bear the risk of these frequent earthquakes by themselves. When moderate earthquakes (with a return period of 100 years) strike, the probable loss is only about 11% of the building value. On the other hand, a rare and stronger earthquake may often incur a loss of 50% or more, thereby rendering the repair uneconomical and necessitating replacement. House owners would obviously be more inclined to pass the risk affiliated to such disastrous consequences to insurers.

It may be noted that risk (defined as the product of probability and consequence in general terms) encompasses all possible hazards. In other words, integration of the loss hazard curve (see Figure 10) represents the total risk due to the structural damage of a URM house. As EAL is the area subtended by the loss hazard curve, it therefore represents an insurer's risk and is directly related to an annual insurance premium for a building, if the consequences of all levels of seismic hazards are to be covered. The contributions of earthquakes of different frequency ranges to the total EAL are also graphically illustrated

in Figure 11. Looking at the trends in Table 13 and Figure 11, it is apparent that the more frequent and smaller events contribute more to the total financial risk, while the large earthquakes lead to much smaller risks due mainly to their very small annual frequency of occurrence (i.e., long return period). For example, among the total EAL of the URM house (i.e., \$8772 per \$1 million replacement value) investigated in this study, 60% corresponds to the risk posed by the frequent but modest size earthquakes with an annual frequency in the range of 0.01 to 0.1 (i.e., with return periods between 10 and 100 years).

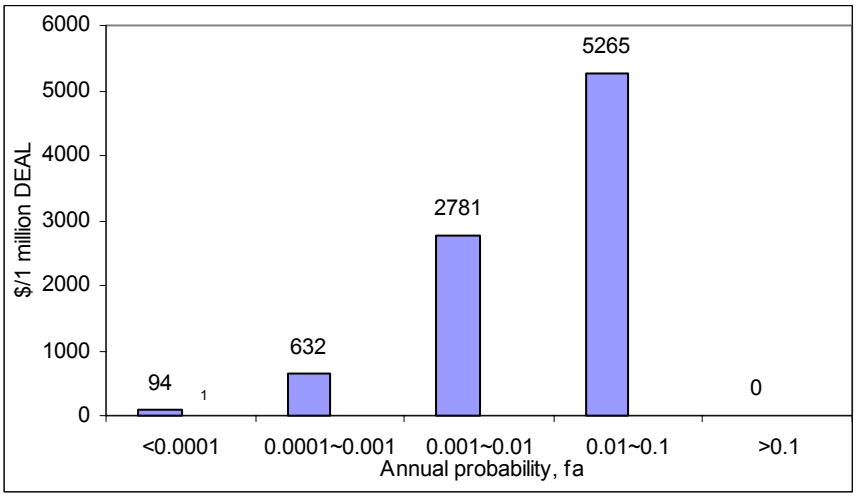

Fig. 11 Annual financial risks due to the earthquakes of different frequency ranges

Although the risk posed by the large and rare events is small, the loss to owners would be untenable if these large events occur. That is why most insurance policies are targeted to cover the rare and bigger hazards. In contrast, the smaller and more frequent events will cause a small loss to the individual owners but a significant collective risk to the insurers. If these frequent hazards are excluded from the insurance policy, the EAL and consequently the annual insurance premium will reduce significantly. From the insurance point-of-view, the owner should ideally carry the risk of these smaller and more frequent events. This can be achieved by setting an appropriate deductible in the insurance policy, which is a minimum loss that has to be borne by the owner in every event. For example, if the overhead costs of the insurer are overlooked and the premiums are assumed to reflect directly the risks, an insurance policy with a \$1,000 deductible on a URM house worth \$1 million implicitly means (see Figure 10) that the owner is completely bearing the consequence of earthquakes of up to approximately 100-year return period.

CONCLUSIONS AND RECOMMENDATIONS

Seismic performance of a typical 2-storey URM house subjected to various ground motions in longitudinal as well as transverse directions has been experimentally investigated in this study. Damage was limited to the toppling of gable walls and to some cracking around window and door piers during the longitudinal shakings. During the shakings in the transverse direction, the second-story face-loaded walls rocked and tended to fail in the out-of-plane direction. The acquired experimental data was processed to generate fragility functions of such URM houses. A finite element analysis has also been performed to assess the strength and dynamic structural characteristics of the experimental model. An amplitude-dependent equivalent viscous damping model, which has been verified by the experimental results, was used to estimate the relationship between the earthquake intensity and the maximum response of the model. The thus-developed response and fragility functions were combined with a code-specified hazard recurrence model and a loss model to calculate the expected annual loss (EAL) of typical URM houses by using a generalized probabilistic financial risk assessment methodology.

Based on the experimental investigations and the financial risk analysis conducted in this study, the following conclusions can be drawn:

1. Gable walls and roofing clay tiles, if present, are the most vulnerable part of an URM house. These could be life threatening even if the house, as a whole, survives an intense shaking. Toppling gable walls and sliding-off roofing tiles could be inhibited by securing them back to the roof structure.

2. Out-of-plane failure of the walls is the major cause behind high damage to the URM houses in shaking. It can be significantly suppressed by increasing the bond strength between the orthogonal walls, thus providing a rigid diaphragm action and reducing their horizontal and vertical spans.
3. Rocking is the most preferred mode of failure in the walls of URM houses because it leads to a stable non-linear response.
4. In-plane damage is mostly concentrated in the zones of high shear stress, notably the bottom storey. Out-of-plane damage occurs mostly in the zones of high response accelerations and starts from the top storey.
5. If a DBE strikes in Wellington, about 30% of the URM houses would either suffer irreparable damage or collapse. However, for an MCE event, about 65% of the URM houses may suffer irreparable damage or collapse, probably leading to the loss of life. It is also found that the URM houses are likely to incur about 37% and 70% losses during a DBE (i.e., an 10%-in-50-years event) and an MCE (i.e., an 2%-in-50-years event), respectively. The EAL of a typical URM house in Wellington is found to be in the order of $8772 per $1 million of the asset value (i.e., around 0.88%). It may be noted that these predictions have been made by using the earthquakes recorded in firm soil in California and hence are valid only if the used records are representative of the earthquake risk and hazard in Wellington.
6. Although the consequence of very large earthquakes might be disastrous, they pose relatively small financial risk due to their very low probability of occurrence. On the other hand, smaller earthquakes may only cause repairable minor–moderate damage to the structures, but these earthquakes pose a big risk as they are likely to strike more often. Calculations have shown that earthquakes with a return period between 10 and 100 years would contribute approximately 60% to the annual financial risk in the case of URM houses.
7. A low-premium insurance policy with an appropriate deductible amount can be set, so that the risk posed by the frequent and moderate earthquakes (which have minor consequences) is borne by the owners, and disastrous consequences of the rare but large earthquakes (which pose relatively smaller risk) are covered by the insurer.

While this study has given an interesting and useful qualitative information on the seismic performance and financial implications of URM houses, the dollar values obtained are only representative and are not precise because of the assumptions and approximations made. Although variations in the capacity and demand and the modelling uncertainty have been quantitatively incorporated in the form of corresponding lognormal coefficients of variation, uncertainties in the assumed loss model have not been accounted for. The values assigned in this study to the loss ratios and drift ratios for different damage states are also somewhat subjective. EAL is sensitive to the loss ratios corresponding to different damage states, especially those for DS2 and DS3. Hence, future studies should try to establish more robust damage and loss models and investigate their uncertainties so that those could be accounted for in estimating the financial risk.

REFERENCES

1. Arya, A.S. (1992). “Masonry and Timber Structures Including Earthquake Resistant Design”, Nem Chand & Brothers, Roorkee.
2. ATC (1996). “Seismic Evaluation and Retrofit of Concrete Buildings: Volume 1”, Report ATC-40, Applied Technology Council, Redwood City, U.S.A.
3. Benedetti, D. and Pezzoli, P. (1996). “Shaking Table Test on Masonry Buildings: Results and Comments”, Joint Report, ISMES, Bergamo, Italy and Politecnico di Milano, Milano, Italy.
4. Bothara, J.K. (2004). “A Shaking Table Investigation on the Seismic Resistance of a Brick Masonry House”, M.E. Thesis, Department of Civil Engineering, University of Canterbury, Christchurch, New Zealand.
5. Bracci, J.M., Reinhorn, A.M. and Mander, J.B. (1992). “Seismic Resistance of Reinforced Concrete Frame Structures Designed only for Gravity, Part I: Design and Properties of One-Third Scale Model Structure”, Technical Report NCEER-92-0027, State University of New York at Buffalo, Buffalo, U.S.A.
6. Bruneau, M. (1994). “State-of-the-Art Report on Seismic Performance of Unreinforced Masonry Buildings”, Journal of Structural Engineering, ASCE, Vol. 120, No. 1, pp. 230–251.

7. Calvi, G.M. and Pavese, A. (1995). "Application of Dynamic Identification Techniques to a Brick Masonry Building Prototype", Proceedings of the 10th European Conference on Earthquake Engineering, Vienna, Austria, Vol. 3, pp. 2413–2418.
8. Chopra, A.K. (1995). "Dynamics of Structures", Prentice-Hall of India Private Limited, New Delhi.
9. Costley, A.C. and Abrams, S.P. (1996). "Dynamic Response of Unreinforced Masonry Buildings with Flexible Diaphragm", Technical Report NCEER-96-0001, State University of New York at Buffalo, Buffalo, U.S.A.
10. Craig, J.I., Goodno, B.J., Towashiraporn, P. and Park, J. (2002). "Fragility Reduction Estimations for URM Buildings Using Response Modification", Proceedings of the 12th European Conference on Earthquake Engineering, London, U.K., Paper No. 805 (on CD).
11. CSI (2002). "SAP 2000—Integrated Software for Structural Analysis & Design, Version 8.0, Analysis Reference Manual", Computers & Structures, Inc., Berkeley, U.S.A.
12. De Felice, G. and Giannini, R. (2000). "Assessment of Vulnerability to Out-of-Plane Collapse of Masonry Walls", Proceedings of the 12th European Conference on Earthquake Engineering, London, U.K., Paper No. 715 (on CD).
13. De Felice, G. and Giannini, R. (2001). "Out-of-Plane Seismic Resistance of Masonry Walls", Journal of Earthquake Engineering, Vol. 5, No. 2, pp. 253–271.
14. Dhakal, R.P. and Mander, J.B. (2005). "Probabilistic Risk Assessment Methodology Framework for Natural Hazards", Report Prepared for Institute of Geological and Nuclear Sciences, Department of Civil Engineering, University of Canterbury, Christchurch, New Zealand.
15. Dhanasekar, M., Page, A.W. and Kleeman, P.W. (1982). "The Elastic Properties of Brick Masonry", International Journal of Masonry Construction, Vol. 2, No. 4, pp. 155–160.
16. Doherty, K.T. (2000). "An Investigation of the Weak Links in the Seismic Load Path of Unreinforced Masonry Buildings", Ph.D. Thesis, Faculty of Engineering, The University of Adelaide, Adelaide, Australia.
17. Doherty, K.T., Griffith, M.C., Lam, N. and Wilson, J. (2002). "Displacement-Based Seismic Analysis for the Out-of-Plane Bending of Unreinforced Masonry Walls", Earthquake Engineering & Structural Dynamics, Vol. 31, No. 4, pp. 833–850.
18. FEMA (1988). "Rapid Visual Screening of Buildings for Potential Seismic Hazards: A Handbook", Report FEMA 154, Federal Emergency Management Agency, Washington, DC, U.S.A.
19. FEMA (2000). "Prestandard and Commentary for the Seismic Rehabilitation of Buildings", Report FEMA 356, Federal Emergency Management Agency, Washington, DC, U.S.A.
20. Griffith, M.C. and Magenes, G. (2003). "Accuracy of Displacement-Based Evaluation of URM Wall Stability", Proceedings of the 7th Pacific Conference on Earthquake Engineering, Christchurch, New Zealand, Paper No. 127 (on CD).
21. Griffith, M.C., Magenes, G., Melis, G. and Picchi, L. (2003). "Evaluation of Out-of-Plane Stability of Unreinforced Masonry Walls Subjected to Seismic Excitation", Journal of Earthquake Engineering, Vol. 7, No. 1 (Special), pp. 141–169.
22. Kennedy, R.P., Cornell, C.A., Campbell, R.D., Kaplan, S. and Perla, H.F. (1980). "Probabilistic Seismic Safety Study of an Existing Nuclear Power Plant", Nuclear Engineering and Design, Vol. 59, No. 2, pp. 315–338.
23. Krawinkler, H. and Miranda, E. (2004). "Performance-Based Earthquake Engineering" in "Earthquake Engineering: From Engineering Seismology to Performance-Based Engineering (edited by Y. Bozorgnia and V.V. Bertero)", CRC Press, Boca Raton, U.S.A.
24. Magenes, G. (2000). "A Method for Pushover Analysis in Seismic Assessment of Masonry Buildings", Proceedings of the 12th World Conference on Earthquake Engineering, Auckland, New Zealand, Paper No. 1866 (on CD).
25. Magenes, G. and Calvi, G.M. (1995). "Shaking Table Tests on Brick Masonry Walls", Proceedings of the 10th European Conference on Earthquake Engineering, Vienna, Austria, Vol. 3, pp. 2419–2424.
26. Magenes, G. and Calvi, G.M. (1997). "In-plane Seismic Response of Brick Masonry Walls", Earthquake Engineering & Structural Dynamics, Vol. 26, No. 11, pp. 1091–1112.

27. Mahaney, J.A., Paret, T.F., Kehoe, B.E. and Freeman, S.A. (1993). "The Capacity Spectrum Method for Evaluating Structural Response during the Loma Prieta Earthquake", Proceedings of the 1993 National Earthquake Conference—Earthquake Hazard Reduction in the Central and Eastern United States: A Time for Examination and Action, Memphis, U.S.A., Vol. 1, pp. 501–510.
28. Martinez, M.E. (2002). "Performance-Based Seismic Design and Probabilistic Assessment of Reinforced Concrete Moment Resisting Frame Structures", M.E. Thesis, Department of Civil Engineering, University of Canterbury, Christchurch, New Zealand.
29. Mengi, Y. and McNiven, H.D. (1986). "A Mathematical Model for Predicting the Non-linear Response of Unreinforced Masonry Walls to In-plane Earthquake Excitation", Report UCB/EERC-86/07, University of California, Berkeley, U.S.A.
30. Moon, F.L., Yi, T.Y. and Leon, R.T. (2006). "Recommendations for Seismic Evaluation and Retrofit of Low-Rise URM Structures", Journal of Structural Engineering, ASCE, Vol. 132, No. 5, pp. 663–672.
31. NIBS (1999). "Earthquake Loss Estimation Methodology HAZUS: Technical Manual", Report prepared for the Federal Emergency Management Agency, National Institute of Building Sciences, Washington, DC, U.S.A.
32. NSET (2000). "Seismic Vulnerability of School Buildings of Kathmandu Valley and Methods for Reducing It", Unpublished Report on the Kathmandu Valley Earthquake Risk Management Project, National Society for Earthquake Technology, Kathmandu, Nepal.
33. NSET-DEQ (2000). "Reconnaissance Report: Chamoli Earthquake of 29th March 1999, India", Joint Study, National Society for Earthquake Technology, Kathmandu, Nepal and Department of Earthquake Engineering, University of Roorkee, Roorkee.
34. NZS (2004). "NZS 1170.5:2004, Structural Design Actions, Part 5: Earthquake Actions—New Zealand", Standards New Zealand, Wellington, New Zealand.
35. NZSEE (1995). "Draft Guidelines for Assessing and Strengthening Earthquake Risk Buildings", New Zealand Society for Earthquake Engineering Inc, Wellington, New Zealand.
36. NZSEE (2006). "Assessment and Improvement of the Structural Performance of Buildings in Earthquake", New Zealand Society for Earthquake Engineering Inc, Wellington, New Zealand.
37. Park, J., Craig, J.I. and Goodno, B.J. (2002). "Simple Nonlinear In-plane Response Models for Assessing Fragility of URM Walls", Proceedings of the Seventh U.S. National Conference on Earthquake Engineering (7NCEE): Urban Earthquake Risk, Boston, U.S.A., Vol. 5, pp. 4319–4328.
38. Paulay, T. and Priestley, M.J.N. (1992). "Seismic Design of Reinforced Concrete and Masonry Buildings", John Wiley & Sons Inc., New York, U.S.A.
39. Pekcan, G., Mander, J.B. and Chen, S.S. (1999). "Fundamental Considerations for the Design of Non-linear Viscous Dampers", Earthquake Engineering & Structural Dynamics, Vol. 28, No. 11, pp. 1405–1425.
40. Peralta, D.F., Hueste, M.B.D. and Bracci, J.M. (2002). "Seismic Performance of Rehabilitated Floor and Roof Diaphragms in Pre-1950s Unreinforced Masonry Buildings", Proceedings of the Seventh U.S. National Conference on Earthquake Engineering (7NCEE): Urban Earthquake Risk, Boston, U.S.A., Vol. 5, pp. 4289–4298.
41. Priestley, M.J.N. (1985). "Seismic Behaviour of Unreinforced Masonry Walls", Bulletin of the New Zealand Society for Earthquake Engineering, Vol. 18, No. 2, pp. 191–205.
42. Qamaruddin, M. and Chandra, B. (1991). "Behaviour of Unreinforced Masonry Buildings Subjected to Earthquakes", The Masonry Society Journal, Vol. 9, No. 2, pp. 47–55.
43. Simsir, C.C., Aschheim, M.A. and Abrams, D.P. (2003). "Influence of Diaphragm Flexibility on the Out-of-Plane Response of Unreinforced Masonry Bearing Walls", Proceedings of the Ninth North American Masonry Conference (9NAMC), Clemson, U.S.A., pp. 779–790.
44. Sobaih, M. (1999). "Seismic Hazard and Countermeasures in Giza City", Bulletin of the International Institute of Seismology and Earthquake Engineering, Vol. 33, pp. 179–207.
45. Tena-Colunga, A. and Abrams, D.P. (1992). "Response of an Unreinforced Masonry Building during the Loma Prieta Earthquake", Structural Research Series 576, Department of Civil Engineering, University of Illinois at Urbana-Champaign, Urbana, U.S.A.

46. Tomazevic, M. (1987). “Dynamic Modelling of Masonry Buildings: Storey Mechanism as a Simple Alternative”, Earthquake Engineering & Structural Dynamics, Vol. 15, No. 6, pp. 731–749.
47. Tomazevic, M. (1996). “Seismic Upgrading of Old Brick-Masonry Urban Houses: Tying of Walls with Steel Ties”, Earthquake Spectra, Vol. 12, No. 3, pp. 599–622.
48. Tomazevic, M. (1999). “Earthquake-Resistant Design of Masonry Buildings”, Imperial College Press, London, U.K.
49. Towashiraporn, P., Park, J., Craig, J.I. and Goodno, B.J. (2002). “Fragility Reduction for URM Building Using Passive Response Modification”, Proceedings of the Seventh U.S. National Conference on Earthquake Engineering (7NCEE): Urban Earthquake Risk, Boston, U.S.A., Vol. 1, pp. 35–44.
50. Yi, T.Y., Moon, F.L. and Leon, R.T. (2006a). “Lateral Load Tests on a Two-Story Unreinforced Masonry Building”, Journal of Structural Engineering, ASCE, Vol. 132, No. 5, pp. 643–652.
51. Yi, T.Y., Moon, F.L. and Leon, R.T. (2006b). “Analyses of a Two-Story Unreinforced Masonry Building”, Journal of Structural Engineering, ASCE, Vol. 132, No. 5, pp. 653–662.